Smart Structures and Systems, *Vol. 18, No. 1 (2016) 155-181*
DOI: http://dx.doi.org/10.12989/sss.2016.18.1.155

Nonlinear modelling and analysis of thin piezoelectric plates: Buckling and post-buckling behaviour

Michael Krommer*, Yury Vetyukov[a] and Elisabeth Staudigl[b]

Institute of Mechanics and Mechatronics, Vienna University of Technology, Getreidemarkt 9, A-1060 Vienna, Austria

(Received September 26, 2015, Revised April 21, 2016, Accepted May 6, 2016)

Abstract. In the present paper we discuss the stability and the post-buckling behaviour of thin piezoelastic plates. The first part of the paper is concerned with the modelling of such plates. We discuss the constitutive modelling, starting with the three-dimensional constitutive relations within Voigt's linearized theory of piezoelasticity. Assuming a plane state of stress and a linear distribution of the strains with respect to the thickness of the thin plate, two-dimensional constitutive relations are obtained. The specific form of the linear thickness distribution of the strain is first derived within a fully geometrically nonlinear formulation, for which a Finite Element implementation is introduced. Then, a simplified theory based on the von Karman and Tsien kinematic assumption and the Berger approximation is introduced for simply supported plates with polygonal planform. The governing equations of this theory are solved using a Galerkin procedure and cast into a non-dimensional formulation. In the second part of the paper we discuss the stability and the post-buckling behaviour for single term and multi term solutions of the non-dimensional equations. Finally, numerical results are presented using the Finite Element implementation for the fully geometrically nonlinear theory. The results from the simplified von Karman and Tsien theory are then verified by a comparison with the numerical solutions.

Keywords: piezoelastic plates; geometrical nonlinearity; buckling and post-buckling behaviour; nonlinear Finite Elements

1. Introduction

Multifunctional materials and their integration into loading bearing systems of structural mechanics are the basis for the development and design of so-called smart or intelligent structures. Such structures are prominent in mechanical, aerospace as well as civil engineering. They react automatically to changing environmental and loading conditions, a feature which is enabled by implementing active or passive control strategies into the smart structures. An introductory overview on these systems and structures can be found in e.g., Crawley (1994) or Tani *et al.* (1998); challenges and opportunities for smart structures are discussed in Liu *et al.* (2005). Typically, smart structures are used to reduce structural vibrations and noise radiation; we refer to

*Corresponding author, Professor, E-mail: michael.krommer@tuwien.ac.at
[a] Ph.D., E-mail: yury.vetyukov@tuwien.ac.at
[b] Ph.D. Student, E-mail: elisabeth.staudigl@tuwien.ac.at

http://www.techno-press.org/?journal=sss&subpage=8 ISSN: 1738-1584 (Print), 1738-1991 (Online)

Nader (2008), Alkhatib and Golnaraghi (2003), Zenz *et al.* (2013) and Nestorović *et al.* (2015) in this later respect. Practical applications range from wind turbines, to rotor blades, to flexible robots, to mention only a few examples.

In the present paper we are not interested in vibrations and vibration reduction of thin piezoelectric plates, but in the study of the buckling and the post-buckling behaviour of such plates. For that reason, we focus on the accurate, yet simple electromechanically coupled modelling of thin piezoelectric plates in the geometrically nonlinear regime, on the reduction of the nonlinear partial differential equations to nonlinear algebraic equations, on the mathematical analysis of the solutions of these equations and on the numerical verification of the results.

The analysis of the buckling and the post-buckling behaviour of thin piezoelectric plates is strongly related to an accurate electromechanically coupled modelling, which on the other hand must be simple enough to enable a mathematical analysis of the nonlinear behaviour. As we consider only thin plates with integrated piezoelectric materials, a modelling as a three-dimensional continuum is neither necessary nor efficient. In such problems it is more efficient to use the classical theories of structural mechanics with their necessary extension to account for integrated piezoelectric materials, which can be used as either actuators or sensors. Such an extension is possible within equivalent single layer theories, see e.g., Krommer (2003), Batra and Vidoli (2009) or Wu and Ding (2015), layer-wise theories or also hybrid theories (Carrera and Boscolo 2007). Typically, a-priori assumptions concerning the thickness distribution of the mechanical and electrical fields are imposed in order to reduce the three-dimensional continuum to a two-dimensional theory of structural mechanics. In the context of geometrically nonlinear theories for plates and shells we refer to the rich literature, e.g., Zheng *et al.* (2004), Tan and Vu-Quoc (2005), Klinkel and Wagner (2006, 2008), Marinković *et al.* (2007, 2008), Lentzen *et al.* (2007) and Arefi and Rahimi (2012). In the present paper an electromechanically coupled equivalent single layer classical lamination theory is presented in either a fully geometrically nonlinear regime or within the framework of the von Karman and Tsien kinematic assumption, see von Karman and Tsien (1941). The later von Karman and Tsien theory is used for the mathematical analysis, whereas the fully geometrically nonlinear theory is used for numerically verifying the results of the mathematical analysis.

Concerning the approximation of the governing nonlinear partial differential equations by ordinary ones, the most commonly used methods are the Rayleigh-Ritz method and the Galerkin procedure (Ziegler 1998) as well as the Finite Element method (Bonet and Wood 2008). In this paper we use the Finite Element method for the fully geometrically nonlinear theory; elements with 4 nodes and 12 degrees of freedom for each node are implemented using bi-cubic shape functions. These elements were previously used for elastic problems by Vetyukov (2014a). For the discretization of the von Karman and Tsien theory a problem-oriented form of the Galerkin procedure using solutions of a corresponding Helmholtz problem with Dirichlet boundary conditions as Ansatz functions results into equations that are particularly advantageous for the mathematical analysis. This solution technique was introduced by Irschik (1986) for the related analysis of the thermoelastic stability of initially curved plates. For an application to shallow shells, see e.g. Heuer and Ziegler (2004). As the piezoelastic problem is similar to the thermoelastic one, this special Galerkin procedure is used to derive a suitable set of nonlinear algebraic equations for quasi-static conditions in the present paper.

Based on the analogy between the thermoelastic problem and the piezoelastic problem (Tauchert 1992) the analysis of the stability of solutions and the post-buckling behaviour for piezoelastic plates follows the one for the case of thermoelastic plates; in particular, as presented

by Irschik (1986). Besides this specific type of analysis, a vast amount of literature concerning thermoelastic stability of thin structures has been published over the last decades; e.g., Ziegler and Rammerstorfer (1989), Tauchert (1991), Hause *et al.* (1998), Heuer and Ziegler (2004) and Stanciulescu *et al.* (2012). In relation with the analysis of buckling and post-buckling of piezoelectric plates we exemplarily refer to Varelis and Saravanos (2002), Jadhav *et al.* (2012), Yaghoobi and Rajabi (2013), Jabbaria *et al.* (2013) and Panahandeh-Shahraki *et al.* (2014), where in the last of these references thermoelastic buckling of laminated piezoelectric composite plates is studied.

In the framework of the solution strategy introduced by Irschik (1986), the equations of the buckling and post-buckling behaviour of a simply supported plate of arbitrary polygonal form are studied in the present paper in a unifying non-dimensional form, where the special geometry of the polygonal plate enters via the eigenvalues of a corresponding linear Helmholtz problem with Dirichlet boundary conditions. This analysis is extended to the case of electromechanically coupled piezoelectric plates discussing also multi term expansions in the Galerkin procedure and the stability of multi term solutions, as well as including transverse force loadings of the plate. Besides the mathematical analysis a numerical Finite Element solution of the fully geometrically nonlinear equations is presented and the results are used for verifying the ones obtained from the mathematical analysis of the von Karman and Tsien theory.

Finally, we mention that the present paper is a substantial extension of the recently published paper by Krommer and Irschik (2015) with respect to: (1) The modelling part of the present paper considers both, the von Karman and Tsien theory and a fully geometrically nonlinear theory; the later was not discussed in Krommer and Irschik (2015). (2) The mathematical analysis of the nonlinear algebraic equations resulting from the von Karman and Tsien theory focuses on two cases; fixed piezoelectric actuation and varying external force loading as well as fixed external force loading and varying piezoelectric actuation. The second case was not studied in Krommer and Irschik (2015). (3) In the second case of fixed external force loading and varying piezoelectric actuation a transcritical bifurcation is found, which was not discussed in Krommer and Irschik (2015). (4) The fully geometrically nonlinear theory is numerically solved with Finite Elements and used to verify the results of the von Karman and Tsien theory.

2. Constitutive modelling

We start our discussion of constitutive equations by introducing an augmented free energy $\Omega(\mathbf{C},\boldsymbol{\mathcal{E}})$ per unit volume in the reference configuration as

$$\Omega(\mathbf{C},\boldsymbol{\mathcal{E}}) = \Phi(\mathbf{C},\boldsymbol{\mathcal{E}}) - \frac{1}{2}\varepsilon_0 J\boldsymbol{\mathcal{E}}\cdot\left(\mathbf{C}^{-1}\cdot\boldsymbol{\mathcal{E}}\right), \tag{1}$$

see e.g., Dorfmann and Ogden (2005). Here, $\mathbf{C}=\mathbf{F}^T\cdot\mathbf{F}$ is the right Cauchy-Green tensor and $\boldsymbol{\mathcal{E}}$ the material electric field vector; the later is related to the spatial electric field vector $\underline{\boldsymbol{\mathcal{E}}}$ by $\boldsymbol{\mathcal{E}}=\mathbf{F}^T\cdot\underline{\boldsymbol{\mathcal{E}}}$. $\Phi(\mathbf{C},\boldsymbol{\mathcal{E}})$ is the free energy, $J=\det\mathbf{F}$ the determinant of the deformation gradient tensor $\mathbf{F}$ and ε_0 the permittivity in vacuum. Then, the symmetric total second Piola-Kirchhoff stress tensor $\mathbf{S}$, which is the sum of the second Piola-Kirchhoff stress tensor $\underline{\mathbf{S}}$ and a second Piola-Kirchhoff type Maxwell stress tensor, $\mathbf{S}_M=\mathcal{D}\boldsymbol{\mathcal{E}}\cdot\mathbf{C}^{-1}-(1/2)\varepsilon_0 J(\boldsymbol{\mathcal{E}}\boldsymbol{\mathcal{E}}\cdot\cdot\mathbf{C}^{-1})\mathbf{C}^{-1}$, and the

material electric displacement vector $\mathcal{D}$ are derived from

$$\mathbf{S} = 2\frac{\partial \Omega}{\partial \mathbf{C}}, \quad \mathcal{D} = -\frac{\partial \Omega}{\partial \mathcal{E}}. \tag{2}$$

These relations are valid for deformable dielectrics in general, and for piezoelectric materials in particular. However, in piezoelectric materials certain approximations can be imposed due to the fact that deformations are only moderately large in these materials.

2.1 Voigt's linearized theory of piezoelasticity

In Voigt's linearized theory of piezoelasticity the augmented free energy is approximated by

$$\Omega(\mathbf{E}, \mathcal{E}) = \Phi(\mathbf{E}, \mathcal{E}) - \frac{1}{2}\varepsilon_0 \mathcal{E} \cdot \mathcal{E}, \tag{3}$$

in which the transformation between the material and the spatial electric field vector and the transformation between volume elements have been neglected in the purely electrical part, $\mathcal{E} \approx \underline{\mathcal{E}}$ and $J \approx 1$. The free energy is formulated in terms of the Green strain tensor $\mathbf{E}$ rather than in terms of the right Cauchy-Green tensor $\mathbf{C} = 2\mathbf{E} + \mathbf{I}$. Now, the free energy is expanded into a Taylor series up to second order terms, see e.g., Kamlah (2001); hence

$$\Phi(\mathbf{E}, \mathcal{E}) = \frac{1}{2}\mathbf{E} \cdot\cdot \mathbb{C} \cdot\cdot \mathbf{E} - \mathcal{E} \cdot \mathbf{e} \cdot\cdot \mathbf{E} - \frac{1}{2}\mathcal{E} \cdot \chi \cdot \mathcal{E}. \tag{4}$$

$\mathbb{C}$, $\mathbf{e}$ and χ are the fourth rank elasticity tensor, the third rank piezoelectric tensor and the second rank susceptibility tensor. Obviously, the derivative of the augmented term with respect to any deformation measure vanishes, and one can compute the total second Piola-Kirchhoff stress tensor $\mathbf{S}$ and the material electric displacement vector $\mathcal{D}$ as

$$\mathbf{S} = \frac{\partial \Omega}{\partial \mathbf{E}} = \mathbb{C} \cdot\cdot \mathbf{E} - \mathbf{e} \cdot \mathcal{E}, \quad \mathcal{D} = -\frac{\partial \Omega}{\partial \mathcal{E}} = \eta \cdot \mathcal{E} + \mathbf{e} \cdot\cdot \mathbf{E}, \tag{5}$$

in which the permittivity tensor $\eta = \varepsilon_0 \mathbf{I} + \chi$ has been introduced. We also note that in classical piezoelectricity we do not distinguish between the total second Piola-Kirchhoff stress tensor and the second Piola-Kirchhoff stress tensor, $\mathbf{S} \equiv \underline{\mathbf{S}}$; hence, both are symmetric.

2.1.1 The plane stress case

As we are interested in thin plates, we impose a plane stress condition on the second Piola-Kirchhoff stress tensor $\mathbf{S} = \mathbf{S}_2 + \boldsymbol{\tau}\mathbf{K} + \mathbf{K}\boldsymbol{\tau} + S_{33}\mathbf{K}\mathbf{K}$; hence, $\mathbf{S} = \mathbf{S}_2$, in which $\mathbf{S}_2$ is the in-plane part of $\mathbf{S}$ and $\mathbf{K}$ is the unit normal vector in thickness direction in the reference configuration. Moreover, owing to the thinness of the plate, the thickness component of the electric displacement vector is assumed to be dominant, $\mathcal{D} = \mathcal{D}_2 + \mathcal{D}_3\mathbf{K} \approx \mathcal{D}_3\mathbf{K}$. Likewise to the stress tensor and the electric displacement vector, we decompose the Green strain tensor and the electric field vector as follows

$$\mathbf{E} = \mathbf{E}_2 + \boldsymbol{\gamma}\mathbf{K} + \mathbf{K}\boldsymbol{\gamma} + E_{33}\mathbf{K}\mathbf{K}\,, \quad \boldsymbol{\mathcal{E}} = \boldsymbol{\mathcal{E}}_2 + \mathcal{E}_3\mathbf{K}. \tag{6}$$

Accounting for the specific form of the material tensors $\mathbb{C}$, $\mathbf{e}$ and $\boldsymbol{\chi}$ for the case of piezoelectric materials, which belong to the crystal class 2mm and which are polarized in the thickness direction, see appendix or Eringen and Maugin (1990), the conditions $\boldsymbol{\tau}=\mathbf{0}$ and $\boldsymbol{\mathcal{D}}_2 = \mathbf{0}$ result into $\boldsymbol{\gamma}=\mathbf{0}$ and $\boldsymbol{\mathcal{E}}_2 = \mathbf{0}$; hence, $\mathbf{E}=\mathbf{E}_2+E_{33}\mathbf{K}\mathbf{K}$ and $\boldsymbol{\mathcal{E}} = \mathcal{E}_3\mathbf{K}$ must hold. Then the augmented free energy becomes

$$\Omega(\mathbf{E}_2, E_{33}, \mathcal{E}_3) = \frac{1}{2}\left(\mathbf{E}_2 + E_{33}\mathbf{K}\mathbf{K}\right)\cdot\cdot\,\mathbb{C}\,\cdot\cdot\left(\mathbf{E}_2 + E_{33}\mathbf{K}\mathbf{K}\right) - \mathcal{E}_3\mathbf{K}\cdot\mathbf{e}\cdot\cdot\left(\mathbf{E}_2 + E_{33}\mathbf{K}\mathbf{K}\right) - \frac{1}{2}\eta_{33}\mathcal{E}_3\mathcal{E}_3. \tag{7}$$

Computing the derivative of the augmented free energy with respect to E_{33} results into S_{33}, which must be zero; hence, from $S_{33}=0$ we compute E_{33} as a function of the plane part of the Green strain tensor $\mathbf{E}_2$ and of $\mathcal{E}_3$. Inserting this result, which we omit for the sake of brevity, into the augmented free energy we have

$$\underline{\Omega}(\mathbf{E}_2, \mathcal{E}_3) = \frac{1}{2}\mathbf{E}_2\,\cdot\cdot\,\underline{\mathbb{C}}\,\cdot\cdot\,\mathbf{E}_2 - \mathcal{E}_3\underline{\mathbf{e}}\,\cdot\cdot\,\mathbf{E}_2 - \frac{1}{2}\underline{\varepsilon}\mathcal{E}_3\mathcal{E}_3, \tag{8}$$

in which $\underline{\mathbb{C}}$, $\underline{\mathbf{e}}$ and $\underline{\varepsilon}$ are effective material tensors for plane stress, which are defined in the appendix. Eventually, we derive the constitutive relations for $\mathbf{S}_2$ and $\mathcal{D}_3$ as

$$\mathbf{S}_2 = \frac{\partial\underline{\Omega}}{\partial\mathbf{E}_2} = \underline{\mathbb{C}}\,\cdot\cdot\,\mathbf{E}_2 - \underline{\mathbf{e}}\mathcal{E}_3\,, \quad \mathcal{D}_3 = -\frac{\partial\underline{\Omega}}{\partial\mathcal{E}_3} = \underline{\varepsilon}\,\mathcal{E}_3 + \underline{\mathbf{e}}\,\cdot\cdot\,\mathbf{E}_2, \tag{9}$$

which are the effective plane stress constitutive relations.

2.2 Structural plate level

On the structural level of thin plates we assume the plane part of the Green strain tensor as a linear function in the thickness direction; hence, $\mathbf{E}_2=\boldsymbol{\varepsilon}+Z\boldsymbol{\kappa}$. This assumption was proven asymptotically by Vetyukov *et al.* (2011) for the case of geometrically linear piezoelectric plates. $\boldsymbol{\varepsilon}$ is an in-plane strain tensor and $\boldsymbol{\kappa}$ a curvature tensor, for which we will discuss specific expressions later on. As $\boldsymbol{\mathcal{D}} = \mathcal{D}_3\mathbf{K}$ holds, the Gauss law of electrostatics simplifies to $\partial_3\mathcal{D}_3 = 0$, which ensures a constant electric displacement $\mathcal{D}_3$ through the thickness h_p of a piezoelectric layer. Therefore, we compute $\mathcal{D}_3$ to

$$\mathcal{D}_3 = \frac{1}{h_p}\int_{h_p}\mathcal{D}_3\,dZ = \underline{\varepsilon}\frac{V}{h_p} + \underline{\mathbf{e}}\,\cdot\cdot\,\boldsymbol{\varepsilon} + Z_m\underline{\mathbf{e}}\,\cdot\cdot\,\boldsymbol{\kappa} = q. \tag{10}$$

Reinserting this result into the constitutive relation for $\boldsymbol{D}_3$ enables us to find $\mathcal{E}_3$ as

$$\mathcal{E}_3 = \frac{V}{h_p} + \left(Z_m - Z\right)\frac{\underline{\underline{\mathbf{e}}}}{\underline{\varepsilon}} \cdot\cdot \boldsymbol{\kappa}. \tag{11}$$

Here, Z_m is the thickness centre of the piezoelectric layer and V the voltage, which is typically applied between the electrodes of a piezoelectric layer; q is a charge per unit area. This result together with $\mathbf{E}_2 = \boldsymbol{\varepsilon} + Z\boldsymbol{\kappa}$ is inserted into the plane part of the augmented free energy finding

$$\begin{aligned}\underline{\Omega}(\boldsymbol{\varepsilon},\boldsymbol{\kappa},V,Z) = {}& \frac{1}{2}\boldsymbol{\varepsilon}\cdot\cdot\underline{\mathbb{C}}\cdot\cdot\boldsymbol{\varepsilon} + \boldsymbol{\varepsilon}\cdot\cdot\left(\underline{\mathbb{C}}Z - \left(Z_m - Z\right)\frac{\underline{\underline{\mathbf{e}}}\,\underline{\underline{\mathbf{e}}}}{\underline{\varepsilon}}\right)\cdot\cdot\boldsymbol{\kappa} \\ & + \frac{1}{2}\boldsymbol{\kappa}\cdot\cdot\left(\underline{\mathbb{C}}Z^2 - \left(Z_m - Z\right)\left(Z_m + Z\right)\frac{\underline{\underline{\mathbf{e}}}\,\underline{\underline{\mathbf{e}}}}{\underline{\varepsilon}}\right)\cdot\cdot\boldsymbol{\kappa} - \frac{V}{h_p}\underline{\mathbf{e}}\cdot\cdot\boldsymbol{\varepsilon} - Z_m\frac{V}{h_p}\underline{\mathbf{e}}\cdot\cdot\boldsymbol{\kappa} - \frac{1}{2}\frac{V}{h_p}\underline{\varepsilon}\frac{V}{h_p}.\end{aligned} \tag{12}$$

Now we assume the plate to be made of n perfectly bonded layers, which may be piezoelectric or otherwise purely elastic, and integrate over the total thickness of the plate to obtain

$$\Omega_2(\boldsymbol{\varepsilon},\boldsymbol{\kappa},V) = \frac{1}{2}\boldsymbol{\varepsilon}\cdot\cdot\mathbb{A}\cdot\cdot\boldsymbol{\varepsilon} + \boldsymbol{\varepsilon}\cdot\cdot\mathbb{B}\cdot\cdot\boldsymbol{\kappa} + \frac{1}{2}\boldsymbol{\kappa}\cdot\cdot\mathbb{D}\cdot\cdot\boldsymbol{\kappa} - \boldsymbol{\varepsilon}\cdot\cdot\sum_{k=1}^{n}\mathbf{p}^k V^k - \boldsymbol{\kappa}\cdot\cdot\sum_{k=1}^{n}\mathbf{m}^k V^k - \frac{1}{2}\sum_{k=1}^{n}c^k (V^k)^2, \tag{13}$$

with the material parameters

$$\begin{aligned}\left(\mathbb{A},\mathbb{B}\right) &= \sum_{k=1}^{n}\int_{h_k}\underline{\mathbb{C}}^k\left(1,Z\right)dZ\,, \quad \mathbf{p}^k = \underline{\mathbf{e}}^k\,, \quad \mathbf{m}^k = Z_m^k\underline{\mathbf{e}}^k\,, \quad c^k = \frac{\underline{\varepsilon}^k}{h^k}\,, \\ \mathbb{D} &= \sum_{k=1}^{n}\int_{h_k} Z\left(\underline{\mathbb{C}}^k Z - \frac{\underline{\mathbf{e}}^k\,\underline{\mathbf{e}}^k}{\underline{\varepsilon}^k}\left(Z_m^k - Z\right)\right)dZ\end{aligned} \tag{14}$$

on the structural plate level. Finally, we introduce stress tensors $\boldsymbol{\tau}$ and $\boldsymbol{\mu}$ for the thin piezoelectric plate according to

$$\boldsymbol{\tau} = \sum_{k=1}^{n}\int_{h_k}\mathbf{S}_2\,dZ\,, \quad \boldsymbol{\mu} = \sum_{k=1}^{n}\int_{h_k}\mathbf{S}_2 Z\,dZ. \tag{15}$$

Inserting the constitutive relations for $\mathbf{S}_2$ given in Eq. (9) together with E_3 from Eq. (11) finds the stress tensors as a function of $\boldsymbol{\varepsilon}$, $\boldsymbol{\kappa}$ and V^k. Alternatively, one can also compute the identical result for $\boldsymbol{\tau}$ and $\boldsymbol{\mu}$ as well as for the charge per unit area q^i from

$$\boldsymbol{\tau} = \frac{\partial\Omega_2}{\partial\boldsymbol{\varepsilon}}\,, \quad \boldsymbol{\mu} = \frac{\partial\Omega_2}{\partial\boldsymbol{\kappa}}\,, \quad q_i = -\frac{\partial\Omega_2}{\partial V^i}, \tag{16}$$

which is straightforward using the augmented free energy from Eq. (13). The result is

$$\begin{bmatrix}\boldsymbol{\tau}\\ \boldsymbol{\mu}\end{bmatrix} = \begin{bmatrix}\mathbb{A} & \mathbb{B}\\ \mathbb{B} & \mathbb{D}\end{bmatrix}\cdot\cdot\begin{bmatrix}\boldsymbol{\varepsilon}\\ \boldsymbol{\kappa}\end{bmatrix} - \begin{bmatrix}\underline{\boldsymbol{\tau}}\\ \underline{\boldsymbol{\mu}}\end{bmatrix}, \quad q_i = c_i V^i + q_i^{\varepsilon} + q_i^{\kappa}, \tag{17}$$

in which we have introduced the abbreviations

$$\underline{\boldsymbol{\tau}} = \sum_{k=1}^{n} \mathbf{p}^k V^k, \quad \underline{\boldsymbol{\mu}} = \sum_{k=1}^{n} \mathbf{m}^k V^k, \quad q_i^{\varepsilon} = \mathbf{p}^i \cdot\cdot \boldsymbol{\varepsilon}, \quad q_i^{\kappa} = \mathbf{m}^i \cdot\cdot \boldsymbol{\kappa}. \tag{18}$$

Our formulation accounts for electromechanical coupling as it includes the piezoelectric material parameters in the definition of the effective bending stiffness tensor $\mathbb{D}$. Such a theory has been introduced by Krommer (2003) for the case of thin plates with small deformations and justified by an asymptotic solution for the linearized three-dimensional theory of piezoelectricity by Vetyukov *et al.* (2011). In the present paper we consider the case of large deformations, such that it remains to define our strain measures $\boldsymbol{\varepsilon}$ and $\boldsymbol{\kappa}$.

3. Geometrically nonlinear thin plates

In the previous section on constitutive modelling we have introduced the plane part of the Green strain tensor as $\mathbf{E}_2 = \boldsymbol{\varepsilon} + Z\boldsymbol{\kappa}$ with the argument that the plate is thin. Although this was proven to be asymptotically correct in Vetyukov *et al.* (2011), we discuss this assumption in some detail and we must define the strain measures $\boldsymbol{\varepsilon}$ and $\boldsymbol{\kappa}$. To succeed with these two tasks, we introduce the position vector of a material point of the plate in the reference configuration as a function of coordinates q^1 and q^2 in a reference plane and of the distance Z from the reference plane. Hence

$$\mathbf{R}_3(q^1, q^2, Z) = \mathbf{R}(q^1, q^2) + Z\mathbf{K}, \tag{19}$$

and we introduce the differential operator for the reference configuration as

$$\nabla_3 = \nabla + \mathbf{K}\,\partial Z. \tag{20}$$

Here, $\nabla \mathbf{R} = \mathbf{A} = \mathbf{I} - \mathbf{K}\mathbf{K}$ holds; $\mathbf{A}$ is the first metric tensor of the reference plane in the reference configuration, $\mathbf{R}$ is the position vector of points in the reference plane, and $\mathbf{K}$ is the unit normal vector of the reference plane. In the deformed configuration the position vector is

$$\mathbf{r}_3(q^1, q^2, Z) = \mathbf{r}(q^1, q^2) + Z\mathbf{k}. \tag{21}$$

$\mathbf{k}$ is the unit normal vector of the deformed reference surface. Basically, we assume the distance from the reference surface conserved and lines normal to the reference plane to remain normal to the reference surface in the course of the deformation. Now we compute the deformation gradient tensor

$$\mathbf{F} = (\nabla_3 \mathbf{r}_3)^T = (\nabla \mathbf{r})^T + Z(\nabla \mathbf{k})^T + \mathbf{K}\mathbf{k} = \mathbf{F}_2 - Z\mathbf{b}_0 + \mathbf{K}\mathbf{k}, \tag{22}$$

with the plane part of the deformation gradient tensor $\mathbf{F}_2 = (\nabla \mathbf{r})^T$ and the material second metric tensor $\mathbf{b}_0 = -(\nabla \mathbf{k})^T$ of the deformed reference surface. The Green strain tensor is then

$$\mathbf{E} = \frac{1}{2}\left(\mathbf{F}^T \cdot \mathbf{F} - \mathbf{I}\right) = \frac{1}{2}\left(\mathbf{F}_2^T \cdot \mathbf{F}_2 - \mathbf{A} - Z\mathbf{F}_2^T \cdot \mathbf{b}_0 - Z\mathbf{b}_0^T \cdot \mathbf{F}_2 + Z^2 \mathbf{b}_0^T \cdot \mathbf{b}_0\right). \tag{23}$$

Furthermore, we note that the plane part of the differential operator for the deformed configuration $\overline{\nabla}$ is related to ∇ via $\nabla = \mathbf{F}_2^T \cdot \overline{\nabla}$; hence, we find

$$\mathbf{b}_0 = -(\nabla \mathbf{k})^T = -(\mathbf{F}_2^T \cdot \overline{\nabla}\mathbf{k})^T = (\mathbf{F}_2^T \cdot \mathbf{b})^T = \mathbf{b} \cdot \mathbf{F}_2, \tag{24}$$

because the second metric tensor $\mathbf{b}$ is symmetric. Eventually, the Green strain tensor can be approximated as

$$\mathbf{E} \approx \frac{1}{2}\left(\mathbf{F}_2^T \cdot \mathbf{F}_2 - \mathbf{A}\right) - Z\mathbf{F}_2^T \cdot \mathbf{b} \cdot \mathbf{F}_2 = \mathbf{E}_2, \tag{25}$$

if we assume the quadratic term in Z negligible. Now, we identify our strain measures in $\mathbf{E}_2 = \boldsymbol{\varepsilon} + Z\boldsymbol{\kappa}$ by comparison; the result is

$$\boldsymbol{\varepsilon} = \frac{1}{2}\left(\mathbf{F}_2^T \cdot \mathbf{F}_2 - \mathbf{A}\right), \quad \boldsymbol{\kappa} = -\mathbf{F}_2^T \cdot \mathbf{b} \cdot \mathbf{F}_2. \tag{26}$$

A plate theory using these strain measures is geometrically exact within the kinematic assumptions that we have made above, see Vetyukov (2014) for the case of purely elastic thin shells. However, the mathematical analysis of the resulting equations is difficult due to the full geometric nonlinearity. Therefore, we will discuss the implementation of a numerical Finite Element scheme in the following.

3.1 Finite Element implementation

In general, the geometrically exact nonlinear plate theory does not allow for analytical solutions; therefore, we implement a Finite Element scheme using the strain measures

$$\boldsymbol{\varepsilon} = \frac{1}{2}\left(\mathbf{F}_2^T \cdot \mathbf{F}_2 - \mathbf{A}\right), \quad \boldsymbol{\kappa} = -\mathbf{F}_2^T \cdot \mathbf{b} \cdot \mathbf{F}_2. \tag{27}$$

These strain measures are used in the augmented free energy $\Omega_2(\boldsymbol{\varepsilon}, \boldsymbol{\kappa}, V^k)$, see Eq. (13), for which we assume the voltages V^k to be given. In case the external forces are conservative, we can introduce a total energy as

$$\Sigma = \Sigma(\mathbf{r}(q^1, q^2), V^k, \mathbf{p}, p_z) = \Sigma^\Omega + \Sigma^{ext}. \tag{28}$$

The total augmented free energy is

$$\Sigma^\Omega = \int_{A_0} \Omega_2\left(\boldsymbol{\varepsilon}, \boldsymbol{\kappa}, V^k\right) dA_0, \tag{29}$$

and Σ^{ext} is the potential energy of the external force loadings $\mathbf{p}$ and p_z. For the Finite Element implementation we use elements with 4 nodes. Each node has 12 mechanical degrees of freedom, which are the position vector $\mathbf{r}$, the base vectors in the deformed configuration $\partial_\alpha \mathbf{r}$ and the vectors of mixed derivatives of the position vector $\partial_{\alpha\beta}\mathbf{r}$, see Vetyukov (2014); ∂_α denotes the partial derivative with respect to q^α, $\alpha = 1,2$. The domain of an element is $\bar{q}^1 \times \bar{q}^2$, in which the local

coordinates $\bar{q}^{\alpha}$ have the range [-1,1]. The position vector within the *j*-th element is approximated as

$$\mathbf{r}^{j}(\bar{q}^{1},\bar{q}^{2})=\sum_{i=1}^{4}S^{i,1}(\bar{q}^{1},\bar{q}^{2})\mathbf{r}^{j,i}+S^{i,2}(\bar{q}^{1},\bar{q}^{2})\partial_{1}\mathbf{r}^{j,i}+S^{i,3}(\bar{q}^{1},\bar{q}^{2})\partial_{2}\mathbf{r}^{j,i}+S^{i,4}(\bar{q}^{1},\bar{q}^{2})\partial_{12}\mathbf{r}^{j,i}. \tag{30}$$

The four bi-cubic shape functions for the node located at $\bar{q}^{1}=\bar{q}^{2}=$ -1 are shown in Fig. 1.

The element degrees of freedom are borrowed from the global vector of degrees of freedom **U**, which contains all mechanical degrees of freedom. The applied voltages at the electroded layers or patches are collected in the vector **V**. For all elements with electrical degrees of freedom the voltages are borrowed from **V**, which ensures the equipotential area condition at the electrodes. As the electric potentials are element wise constant, no approximation is needed for the voltages within the element. Finally, we seek for an extremum of the total energy functional

$$\Sigma=\Sigma^{\Omega}+\Sigma^{ext}\quad\rightarrow\quad\text{Extremum}, \tag{31}$$

from which nonlinear algebraic equations are derived to compute equilibrium points numerically.

3.2 von Karman and Tsien equations

Besides the numerical solution to the fully geometrically nonlinear theory, we are also interested in the mathematical analysis of the studied plate problems to give a better insight into the nonlinear behaviour of thin piezoelectric plates. To enable the latter, the much simpler von Karman and Tsien theory (von Karman and Tsien 1941) is introduced in this section. In the von Karman and Tsien theory the displacement vector is approximated by

$$\mathbf{u}_{3}(q^{1},q^{2},Z)=\mathbf{r}(q^{1},q^{2})-\mathbf{R}(q^{1},q^{2})+Z\left(\mathbf{k}-\mathbf{K}\right)\approx\mathbf{u}(q^{1},q^{2})+w(q^{1},q^{2})\mathbf{K}-Z\nabla w(q^{1},q^{2}), \tag{32}$$

in which $\mathbf{u}(q^{1},q^{2})$ is the in-plane displacement vector of material points of the reference surface and $w(q^{1},q^{2})$ is the out-of-plane displacement of these points. Then, the strain measures are approximated by

$$\boldsymbol{\varepsilon}=\frac{1}{2}\left(\nabla\mathbf{u}+(\nabla\mathbf{u})^{T}+\nabla w\nabla w\right),\quad\boldsymbol{\kappa}=-\nabla\nabla w. \tag{33}$$

The balance equations and the boundary conditions of the von Karman and Tsien plate theory for moderately large deformation can now be easily derived from a variational principle such as Hamilton's principle. The result for the balance equations is

$$\nabla\cdot\boldsymbol{\tau}+\mathbf{p}=P\ddot{\mathbf{u}}\quad\text{and}\quad\nabla\cdot\nabla\cdot\boldsymbol{\mu}+\nabla\cdot\left(\boldsymbol{\tau}\cdot\nabla w\right)+p_{z}=P\ddot{w}. \tag{34}$$

The balance equations must hold in the plane domain A_0, which constitutes the reference surface of the thin plate. In Eq. (34) $\boldsymbol{\tau}$ and $\boldsymbol{\mu}$ are the two stress tensors we have already introduced, and which we will denote as the in-plane force tensor and the moment tensor in the following. **p** and p_z denote the external distributed in-plane and transverse forces and P stands for the linear inertia. All entities are assumed as functions of the Lagrangian position vector $\mathbf{R}(q^{1},q^{2})$ of the

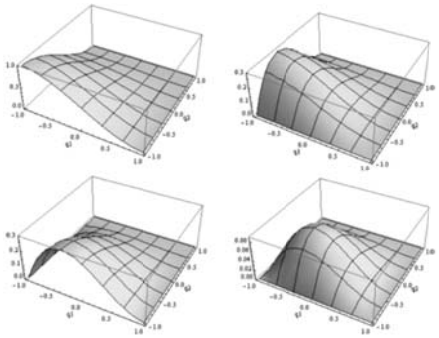

Fig. 1 Shape functions

reference surface. The boundary conditions can be written in a variational form as

$$\begin{aligned}&\left(\boldsymbol{\tau}\cdot\mathbf{n}-\bar{\mathbf{n}}\right)\cdot\delta\mathbf{u}=\mathbf{0},\left(\left(\boldsymbol{\mu}\cdot\mathbf{n}\right)\cdot\mathbf{n}-\bar{m}\right)\delta\left(\nabla w\cdot\mathbf{n}\right)=0,\\&\left((\nabla\cdot\boldsymbol{\mu})\cdot\mathbf{n}+\nabla\left[\left(\boldsymbol{\mu}\cdot\mathbf{n}\right)\cdot\mathbf{s}\right]\cdot\mathbf{s}+\left(\boldsymbol{\tau}\cdot\nabla w\right)\cdot\mathbf{n}-\bar{q}\right)\delta w=0.\end{aligned}\tag{35}$$

These boundary conditions must hold along the boundary curve C_0 of the plane domain A_0. $\mathbf{n}$ and $\mathbf{s}$ are the unit normal and tangential vector of C_0, respectively. Entities with an overbar are prescribed forces and moments at the boundary. The constitutive relations for $\boldsymbol{\tau}$ and $\boldsymbol{\mu}$ have already been derived, see Eq. (17).

3.2.1 Berger approximation

In order to further simplify our equations we apply the Berger approximation, see Berger (1955). For that sake, we assume plates with boundaries that are prevented from any in-plane motion, $\mathbf{u}=\mathbf{0}$, and for which the in-plane forces vanish, $\mathbf{p}=\mathbf{0}$. Then, it is accepted to assume the in-plane inertia to be negligible. Furthermore, we consider a symmetric lamination scheme, $\mathrm{B}=\mathbf{0}$, and every layer to be transversally isotropic with respect to the reference surface; this allows us to write the constitutive relations for the stress tensors as

$$\begin{aligned}\boldsymbol{\tau}&=\mathbb{A}\cdot\cdot\boldsymbol{\varepsilon}-\underline{\boldsymbol{\tau}}=A\nu_A\mathbf{A}tr\boldsymbol{\varepsilon}+A\left(1-\nu_A\right)\boldsymbol{\varepsilon}-\mathbf{A}\underline{\tau},\\\mu&=\mathbb{D}\cdot\cdot\boldsymbol{\kappa}-\underline{\boldsymbol{\mu}}=D\nu_D\mathbf{A}tr\boldsymbol{\kappa}+D\left(1-\nu_D\right)\boldsymbol{\kappa}-\mathbf{A}\underline{\mu}.\end{aligned}\tag{36}$$

Note that $\mathbf{A}=\mathbf{I}-\mathbf{KK}$ is the first metric tensor of the reference plane in the reference configuration. For details concerning the computation the effective actuation $\underline{\tau}$ and $\underline{\mu}$ and of the plate material parameters A, D, ν_A and ν_D, we refer to Krommer (2003); for completeness, the formulas are also given in the Appendix. Due to the isotropic constitutive relations on the plate level, we can decompose the augmented free energy from Eq. (13) into a membrane energy U_{Sm}, a bending energy U_{Sb} and a purely electrical part, $\Omega=U_{Sm}+U_{Sb}+\Omega_{el}$. The membrane energy is a function of the first and the second invariant of the strain measure $\boldsymbol{\varepsilon}$ and of the electric field E_3. Here, the Berger approximation (Berger 1955) can be applied, which assumes the second invariant

of $\boldsymbol{\varepsilon}$ to be negligible compared to the square of the first invariant. This approximation was also used by Irschik (1986) for thermoelastic plates and by Heuer (1994) for thermoelastic shallow shells. With the Berger approximation, the augmented free energy contains the terms

$$\begin{aligned} \Omega_{el} &= -\frac{1}{2}\sum_{k=1}^{n} c^k (V^k)^2 \,, \quad U_{Sm} = \frac{1}{2}\int_{A_0} \Big(A(tr\boldsymbol{\varepsilon})^2 - 2\underline{\tau} tr\boldsymbol{\varepsilon} \Big) dA_0 , \\ U_{Sb} &= \frac{1}{2}\int_{A_0} \Big(D\Big((tr\boldsymbol{\kappa})^2 - 2(1-\nu_D) II_{\kappa} \Big) - 2\underline{\mu} tr\boldsymbol{\kappa} \Big) dA_0 . \end{aligned} \tag{37}$$

Using Hamilton's principle we derive the balance equations within the assumptions we have made; they read

$$\nabla \tau_B = 0 \quad \text{and} \quad \Delta\Big(D\Delta w - \tau_B w + \underline{\mu} \Big) + P\ddot{w} = p_z , \tag{38}$$

with the so-called Berger force τ_B

$$\tau_B = A tr\boldsymbol{\varepsilon} - \underline{\tau} . \tag{39}$$

Δ is the plane Laplace operator. Taking the boundaries to be simply supported and A_0 to be polygonal, the boundary conditions are

$$\mathbf{u} = \mathbf{0} \,, \quad D\Delta w - \tau_B w + \underline{\mu} = 0 \quad \text{and} \quad w = 0 . \tag{40}$$

From the first balance relation $\nabla \tau_B = 0$ we conclude that τ_B must be constant in the domain of the plate. Using the boundary condition $\mathbf{u}=\mathbf{0}$, integration over the plate domain A_0 finds the Berger force as

$$\tau_B = -A\frac{1}{2A_0}\int_{A_0} w\Delta w \, dA_0 - \overline{\tau} \quad \text{with} \quad \overline{\tau} = \frac{1}{A_0}\int_{A_0} \underline{\tau} \, dA_0 . \tag{41}$$

Therefore, we have reduced the von Karman and Tsien equations to a single fourth order nonlinear partial differential equation with corresponding boundary conditions. The bracketed term in the differential equation is denoted as a Marcus moment $\mu_M = D\Delta w - \tau_B w + \underline{\mu}$, see Marcus (1932), which allows us to write the initial-boundary-value problem as

$$\Delta\mu_M + P\ddot{w} = p_z \,, \quad D\Delta w - \tau_B w + \underline{\mu} = \mu_M , \tag{42}$$

with the boundary conditions

$$\mu_M = 0 \,, \quad w = 0 . \tag{43}$$

We now proceed to the approximate solution of this initial-boundary-value problem.

3.3 Galerkin procedure

We solve the second order problem $D\Delta w - \tau_B w + \underline{\mu} = \mu_M$ with the boundary condition $w=0$ by using the Galerkin procedure, see Ziegler (1998). As basis functions for the Ritz-Ansatz we use the orthonormal eigenfunctions of the Helmholtz eigenvalue problem with homogenous Dirichlet boundary conditions, which is defined within the same polygonal domain A_0 as the plate; hence, the basis functions are computed from

$$A_0 : \Delta W_k + \alpha_k W_k = 0\,, \quad C_0 : W_k = 0, \tag{44}$$

in which α_k are the Helmholtz eigenvalues. The Ritz-Ansatz

$$w(\mathbf{R},t) = \sum_{k=1}^{n} W_k(\mathbf{R}) w_k(t), \tag{45}$$

which satisfies the boundary condition $w=0$, is inserted into the differential equation resulting into an error e^*

$$e^* = -D\sum_{k=1}^{n} \alpha_k W_k w_k(t) - \tau_B \sum_{k=1}^{n} W_k w_k(t) - \left(\mu_M - \underline{\mu}\right). \tag{46}$$

We find $i=1,\ldots,n$ nonlinear algebraic equations from the orthogonality relations

$$\int_{A_0} e^* W_i \, dA_0 = 0. \tag{47}$$

Due to the orthonormality of the Helmholtz eigenfunctions W_k these equations are

$$D\alpha_i w_i + \tau_B w_i = \underline{\mu}_i - \mu_{Mi}, \tag{48}$$

with the expansion coefficients of $\underline{\mu}$ and μ_M:

$$\underline{\mu}_i = \int_{A_0} \underline{\mu} W_i \, dA_0 \quad \text{and} \quad \mu_{Mi} = \int_{A_0} \mu_M W_i \, dA_0. \tag{49}$$

Next, the Ritz-Ansatz is inserted into the definition of the Berger force from Eq. (41) finding

$$\tau_B = \frac{A}{2A_0} \sum_{k=1}^{n} \alpha_k w_k^2 - \overline{\tau}. \tag{50}$$

It remains to compute the coefficients μ_{Mi} from the second problem $\Delta\mu_M + P\ddot{w} = p_z$ with homogenous Dirichlet boundary conditions $\mu_M=0$. Again, we use the Galerkin procedure with the same Ansatz-functions

$$\mu_M(\mathbf{R},t) = \sum_{k=1}^{n} W_k(\mathbf{R}) \mu_{Mk}(t). \tag{51}$$

In this problem the error e^{μ} is

$$e^{\mu} = -\sum_{k=1}^{n} \alpha_k W_k \mu_{Mk}(t) + P \sum_{k=1}^{n} W_k \ddot{w}_k(t) - p_z, \tag{52}$$

and the Galerkin procedure finds

$$\mu_{Mi} = -\frac{p_i}{\alpha_i} + \frac{P}{\alpha_i} \ddot{w}_i \quad \text{with} \quad p_i = \int_{A_0} p_z W_i \, dA_0. \tag{53}$$

Finally, we combine the equations and find a system of nonlinear ordinary differential equations

$$\frac{P}{\alpha_i} \ddot{w}_i + w_i \left(\left(D\alpha_i - \bar{\tau} \right) + \frac{A}{2A_0} \sum_{k=1}^{n} \alpha_k w_k^2 \right) = \frac{p_i}{\alpha_i} + \underline{\mu}_i. \tag{54}$$

3.3.1 Non-dimensional formulation

We now introduce a non-dimensional formulation with the non-dimensional parameters

$$\tilde{w}_i = \frac{w_i}{h}, \tilde{\alpha}_i = \alpha_i h^2, \tilde{\ell} = \frac{h^2}{D} \frac{A}{2A_0}, \tilde{\tau} = \frac{h^2}{D} \bar{\tau} \tilde{\mu}_i = \frac{h}{D} \underline{\mu}_i, \tilde{p}_i = \frac{h_3}{D} p_i, \tilde{m}_i = \frac{ph^4}{\tilde{\ell} D \tilde{\alpha}_i^2} \tag{55}$$

which can be written as

$$\tilde{m}_i \ddot{\tilde{w}}_i + \tilde{w}_i \left(\tilde{\tau}_i + \frac{1}{\tilde{\alpha}_i} \sum_{k=1}^{n} \tilde{\alpha}_k \tilde{w}_k^2 \right) = \tilde{\kappa}_i. \tag{56}$$

Here, the new entities

$$\tilde{\tau}_i = \frac{1}{\tilde{\ell}} \left(1 - \frac{\tilde{\tau}}{\tilde{\alpha}_i} \right) \quad \text{and} \quad \tilde{\kappa}_i = \frac{\tilde{p}_i + \tilde{\alpha}_i \tilde{\mu}_i}{\tilde{\ell} \tilde{\alpha}_i^2} \tag{57}$$

have been introduced. The piezoelectric actuation enters by means of $\tilde{\tau}$ and $\tilde{\mu}_i$, and the external force loading p_z by means of $\tilde{p}_i$.

4. Analysis and discussion

In the analysis, we only consider situations, for which a voltage is applied to all piezoelectric actuators. Without a loss of generality, we restrict ourselves to problems with only one piezoelectric layer, such that only one actuation voltage V is present in the formulation. Moreover, we only study the static case in the present paper; hence, all $\tilde{m}_i$ are zero and we have the system of nonlinear algebraic equations

$$\tilde{w}_i\left(\tilde{\tau}_i+\frac{1}{\tilde{\alpha}_i}\sum_{k=1}^{n}\tilde{\alpha}_k\tilde{w}_k^2\right)=\tilde{\kappa}_i\,,\quad i=1,...,n. \tag{58}$$

4.1 Single term expansion for the right hand side

We start assuming a single term expansion for the right hand side, $\tilde{\kappa}_1 \neq 0$. In this case a possible solution is $\tilde{w}_1 \neq 0$ and $\tilde{w}_k = 0$ for $k \neq 1$, such that we have the single cubic equation

$$\tilde{w}_1^3+\tilde{\tau}_1\tilde{w}_1-\tilde{\kappa}_1=0; \tag{59}$$

all the other equations $i=2,\ldots,n$ are identically satisfied. This equation represents a cusp catastrophe, see e.g., Troger and Steindl (1991). In contrast to the classical equation, in which $\tilde{\tau}_1$ and $\tilde{\kappa}_1$ are independent, we are dealing with a problem, for which both of these two entities depend on the voltage, $\tilde{\tau}_1 = \tilde{\tau}_1(V)$ and $\tilde{\kappa}_1 = \tilde{\kappa}_1(V)$. In particular, $\tilde{\kappa}_1$ can be decomposed into a part due to the external forces and a part resulting from the actuation; hence, we have

$$\tilde{\kappa}_1=\tilde{\kappa}_{V1}(V)+\tilde{\kappa}_{p1}. \tag{60}$$

As the first part in this decomposition depends on the voltage V, we can easily establish a relation between $\tilde{\tau}_1(V)$ and $\tilde{\kappa}_1(V)$. With the relation $\tilde{\tau} = \tilde{\beta}_\tau V$, in which $\tilde{\beta}_\tau$ is a proportionality factor, we compute $\tilde{\tau}_1$ as

$$\tilde{\tau}_1=\frac{1}{\tilde{\ell}}\left(1-\frac{\tilde{\tau}}{\tilde{\alpha}_1}\right)=\frac{1}{\tilde{\ell}}\left(1-\frac{\tilde{\beta}_\tau}{\tilde{\alpha}_1}V\right). \tag{61}$$

Likewise, $\tilde{\kappa}_{V1} = \tilde{\beta}_{\kappa,1}V$ with another proportionality factor $\tilde{\beta}_{\kappa,1}$, must hold as well. Then we find the relation

$$\tilde{\kappa}_{V1}=\tilde{\alpha}_1\left(1-\tilde{\ell}\tilde{\tau}_1\right)\frac{\tilde{\beta}_{\kappa,1}}{\tilde{\beta}_\tau}=\tilde{\kappa}_{V1}(\tilde{\tau}_1), \tag{62}$$

which we insert into the cubic equation to obtain

$$\tilde{w}_1^3+\tilde{\tau}_1\tilde{w}_1-\tilde{\kappa}_{V1}(\tilde{\tau}_1)-\tilde{\kappa}_{p1}=0. \tag{63}$$

In the present problem the actuation voltage produces both, an in-plane actuation and an actuation moment; hence, we have a different problem compared to e.g. Irschik (1986) and Heuer and Ziegler (2004), where only an in-plane actuation was induced due to temperature. In our case the problem is not symmetric. For the following analysis we use the parameters

$$\tilde{\alpha}_1=0.000513219\,,\quad \tilde{\ell}=3.79544\quad\text{and}\quad \frac{\tilde{\beta}_{\kappa,1}}{\tilde{\beta}_\tau}=\tilde{\lambda}_1=-127.412. \tag{64}$$

These parameters are computed for a bimorph plate with two identical piezoelectric layers. One is short-circuited and a voltage is applied to the other one. The dimensions of the rectangular plate are a×b×h=1 m×1.5 m×0.006 m. The numerical results for the equilibrium points are plotted in Fig. 2(a). The thick line is an equilibrium branch for the specific external loading $\tilde{\kappa}_{p1} = 0.0807$, which is shown in the $(\tilde{\tau}_1, \tilde{w}_1)$-plane in Fig. 2(b) together with some neighbouring equilibrium branches for slightly different values of $\tilde{\kappa}_{p1}$. In this graph stable (solid line) and unstable (dashed line) branches are shown; to determine the stability of equilibrium points we use the Dirichlet stability criterion for conservative systems, see Ziegler (1998), in this paper.

We can see that in the vicinity of the bifurcation point

$$\tilde{w}_1 = 0.2482\,, \quad \tilde{\kappa}_{p1} = 0.0807 \quad \text{and} \quad \tilde{\tau}_1 = -0.1850, \tag{65}$$

we have a transcritical bifurcation. One should however be careful concerning the stability of the equilibrium branches, because it is well known that the stability in such problems can only be correctly determined by considering a multi term solution rather than a single term solution, see Ashwell (1962), Irschik (1986) and Heuer and Ziegler (2004).

4.1.1 Double term solution

In order to discuss the stability of the equilibrium branches for the single term expansion of the right hand side, we study multi term solutions next. Hence, we have

$$\tilde{w}_1\left(\tilde{\tau}_1 + \frac{1}{\tilde{\alpha}_1}\sum_{k=1}^{n}\tilde{\alpha}_k\tilde{w}_k^2\right) = \tilde{\kappa}_1 \quad \text{and} \quad \tilde{w}_i\left(\tilde{\tau}_i + \frac{1}{\tilde{\alpha}_i}\sum_{k=1}^{n}\tilde{\alpha}_k\tilde{w}_k^2\right) = 0\,, \quad i \neq 1. \tag{66}$$

One can see that only double term solutions with $\tilde{w}_1 \neq 0$, $\tilde{w}_i \neq 0$, but $\tilde{w}_k = 0$ for $k \neq 1, i$ exist. In this case the bracketed term in the second equation must vanish

$$-\tilde{\alpha}_i\tilde{\tau}_i = \left(\tilde{\alpha}_1\tilde{w}_1^2 + \tilde{\alpha}_i\tilde{w}_i^2\right), \tag{67}$$

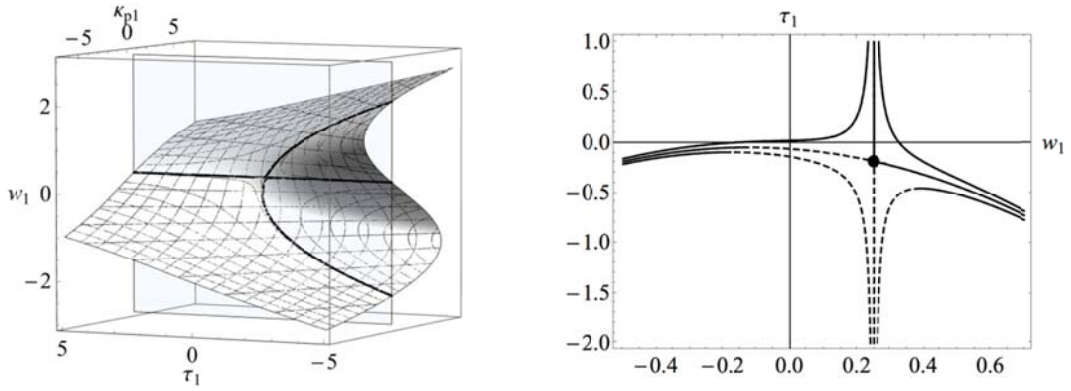

(a) 3D equilibrium chart for the single term solution (b) $(\tilde{\tau}_1, \tilde{w}_1)$-curve with transcritical bifurcation

Fig. 2 Equilibrium charts for the single term solution

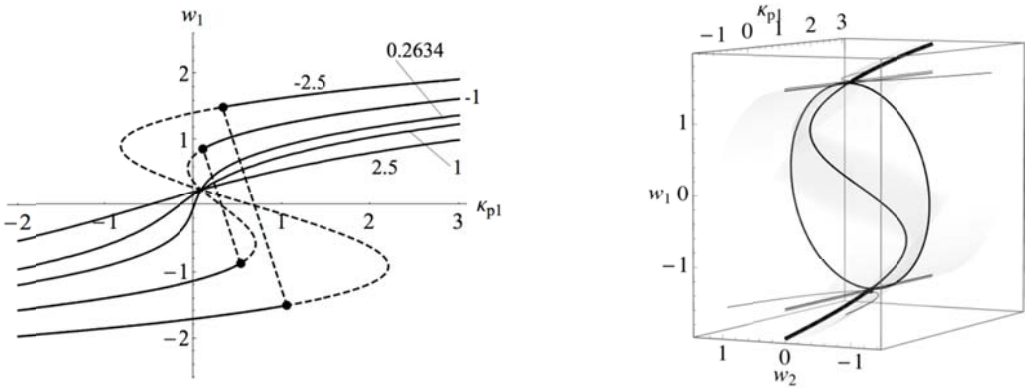

(a) $(\tilde{w}_1, \tilde{\kappa}_{p1})$-curves for different $\tilde{\tau}_1$ (b) 3D Equilibrium chart for $\tilde{\tau}_1 = -2.5$

Fig. 3 Equilibrium charts for the double term solution for different $\tilde{\tau}_1$

which is possible for only one specific $i \neq 1$, if all $\tilde{\alpha}_i \tilde{\tau}_i$ for $i > 1$ are different; in this paper, we only study such cases. In particular, we consider the case of $\tilde{w}_2 \neq 0$, because it is known from our previous work, see Krommer and Irschik (2015), that this is the case that determines the stability of $\tilde{w}_1$. Eq. (67) with $i = 2$ represents an ellipse in the $(\tilde{w}_1, \tilde{w}_2)$-plane for the case $\tilde{\alpha}_2 \tilde{\tau}_2 < 0$. In this case Eq. (67) can be plugged into the equation for $\tilde{w}_1$; this results into

$$\tilde{w}_1 \left(\tilde{\tau}_1 - \frac{\tilde{\alpha}_2}{\tilde{\alpha}_1} \tilde{\tau}_2 \right) = \tilde{\kappa}_{V1} + \tilde{\kappa}_{p1}. \tag{68}$$

Using the definition of $\tilde{\tau}_1$, $\tilde{\tau}_2$ and $\tilde{\kappa}_{V1}(\tilde{\tau}_1)$ a linear equation is found

$$\left[\frac{1}{\tilde{\ell}} \left(1 - \frac{\tilde{\alpha}_2}{\tilde{\alpha}_1} \right) \right] \tilde{w}_1 + \left[\tilde{\alpha}_1 \tilde{\lambda}_1 \tilde{\ell} \right] \tilde{\tau}_1 - \tilde{\kappa}_{p1} = \tilde{\alpha}_1 \tilde{\lambda}_1. \tag{69}$$

This solution for $\tilde{w}_1$ with $\tilde{w}_2 \neq 0$ only exits for $\tilde{\alpha}_2 \tilde{\tau}_2 < 0$, which is satisfied, if $\tilde{\tau}_2 < 0$ or in terms of $\tilde{\tau}_1$ for

$$\tilde{\tau}_1 < \frac{1}{\tilde{\ell}} \left(1 - \frac{\tilde{\alpha}_2}{\tilde{\alpha}_1} \right) < 0. \tag{70}$$

In order to compute numerical solutions, we use again the bimorph plate and note the second Helmoltz eigenvalue $\tilde{\alpha}_2$=0.00098696; then $\tilde{\tau}_1$<-0.2432 must hold for the existence of solutions with $\tilde{w}_2 \neq 0$.

Numerical results are presented in Fig. 3. Dashed (or thin solid) lines represent unstable branches and solid (or thick solid) lines stable ones. In Fig. 3(a) equilibrium branches are shown in the $(\tilde{w}_1, \tilde{\kappa}_{p1})$-plane for different values of $\tilde{\tau}_1$; in particular, for $\tilde{\tau}_1$=(-2.5, -1, 0.2634, 1, 2.5). In Fig. 3(b) the equilibrium branches for $\tilde{\tau}_1$=-2.5 are shown in the $(\tilde{w}_1, \tilde{w}_2, \tilde{\kappa}_{p1})$-space.

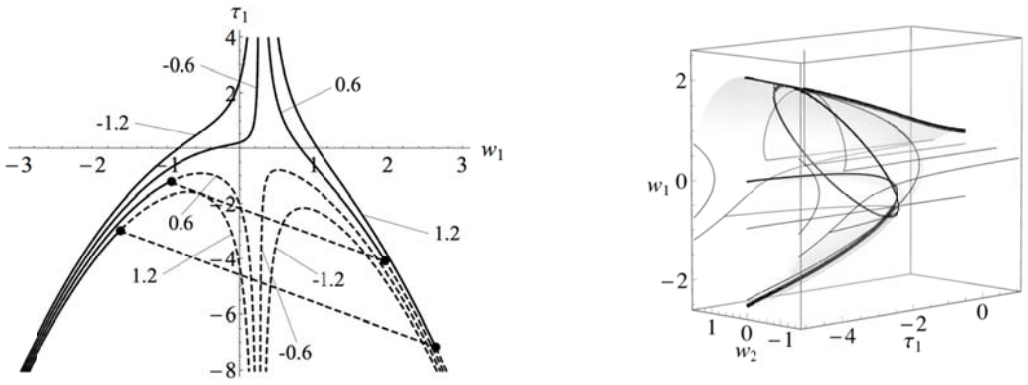

(a) $(\tilde{\tau}_1, \widetilde{w}_1)$-curves for different $\tilde{\kappa}_{p1}$ (b) 3D Equilibrium chart for $\tilde{\kappa}_{p1} = 0.6$

Fig. 4 Equilibrium charts for the double term solution for different $\tilde{\kappa}_{p1}$

From Fig. 3(a) one can see that for $\tilde{\tau}_1$>0 no unstable equilibrium branches are obtained; in contrast for $\tilde{\tau}_1$<0 unstable branches exist. In particular, one can see that due to the existence of solutions with $\widetilde{w}_2 \neq 0$ for $\tilde{\tau}_1$<-0.2432 the single term solution for $\widetilde{w}_1$ becomes unstable at the critical values

$$\tilde{\kappa}_{p1}^{crit,sb} = \pm\left(\tilde{\tau}_1 - \frac{\tilde{\alpha}_2}{\tilde{\alpha}_1}\tilde{\tau}_2\right)\sqrt{-\frac{\tilde{\alpha}_2}{\tilde{\alpha}_1}\tilde{\tau}_2} - \tilde{\alpha}_1\left(1-\tilde{\ell}\tilde{\tau}_1\right)\tilde{\lambda}_1, \tag{71}$$

see Krommer and Irschik (2015) for a derivation. At these equilibrium points a bifurcation to equilibrium branches with $\widetilde{w}_2 \neq 0$ occurs, which are unstable as well. This instability is called snap buckling in the literature, see Heuer *et al.* (1993), and it occurs due to unstable mode jumping. This phenomenon is shown in Fig. 3(b), in which the ellipse for solutions with $\widetilde{w}_2 \neq 0$ can be observed. Besides the behavior for fixed $\tilde{\tau}_1$, we are also interested in the one for fixed $\tilde{\kappa}_{p1}$. The results for the equilibrium branches in the $(\tilde{\tau}_1, \widetilde{w}_1)$-plane for $\tilde{\kappa}_{p1}$=(-1.2, -0.6, 0.6, 1.2) are shown in Fig. 4(a). For negative $\tilde{\kappa}_{p1}$ we have two separated equilibrium branches; one is stable (solid lines) and one is unstable (dashed lines). This result is different from the one for the single term solution, for which the unstable branch present in the double term solution is composed of a stable branch and a connected unstable branch. For positive $\tilde{\kappa}_{p1}$ we have three equilibrium branches. Two of them with $\widetilde{w}_2 = 0$, which are connected to each other by the third branch with $\widetilde{w}_2 \neq 0$; this third branch is unstable and the equilibrium points, at which the third branch bifurcates from the other two branches, separate the stable and unstable branches for the two branches with $\widetilde{w}_2 = 0$. The bifurcation in this problem results again from unstable mode jumping. Fig. 4(b) shows the equilibrium branches for $\tilde{\kappa}_{p1} = 0.6$ in the $(\widetilde{w}_1, \widetilde{w}_2, \tilde{\tau}_1)$-space, in which the three branches can be seen (thin solid lines represent unstable equilibrium points).

The behaviour for $\tilde{\kappa}_{p1} > 0$ is quite interesting, as the positive $\widetilde{w}_1$, which we have for a positive force loading with a zero actuation, $\tilde{\tau}_1$=0.264, is first increased, if the actuation is decreased $\tilde{\tau}_1$<0.264; yet, at a critical value of the actuation $\tilde{\tau}_1$, which is negative, the equilibrium becomes unstable and a snap buckling to $\widetilde{w}_1 < 1$ occurs. In the following we will verify this

behavior with Finite Element results using the exact geometrically nonlinear formulation. For that sake, we first have to discuss a problem with a multi term expansion of the right hand side in the next section.

4.2 Double term expansion for the right hand side

In most practical problems a single term expansion of the right hand side is not sufficient. E.g., in case of the plate shown in Fig. 5 the piezoelectric actuation results into a right hand side, for which all the $\tilde{\kappa}_{Vi}$ belonging to symmetric Helmholtz eigenmodes are non zero. We study such a case in this section. As an underlying physical plate we use the one from the previous examples, which is the one shown in Fig. 5.

Besides the piezoelectric actuation, a constant pressure is applied, from which we also obtain all symmetric $\tilde{\kappa}_{pi}$ non-zero. For this plate, for which both layers are made of *PZT-5A*, the stiffness and actuation parameters are given in Table 1 (the 3D material parameters can be found in the Appendix); we note that the bottom layer is not used as an actuator, but it is assumed to be short-circuited. With the physical dimensions $a \times b \times h = 1\ \mathrm{m} \times 1.5\ \mathrm{m} \times 0.006\ \mathrm{m}$, we can compute the non-dimensional parameters needed for the analysis; these are given in Table 2.

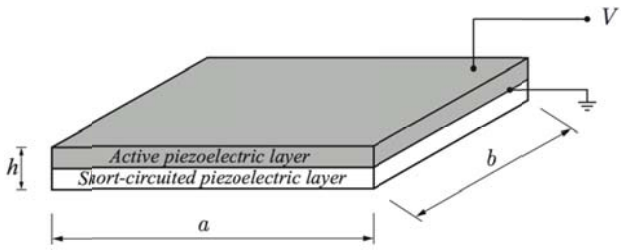

Fig. 5 Plate geometry

Table 1 Stiffnesses and actuation in-plane force and moment for the plate

A	D	$\underline{\tau} / V$	$\underline{\mu} / V$
$4.20322 \times 10^{8}\mathrm{Nm}^{-1}$	1328.93Nm	$-16.1641\mathrm{Nm}^{-1}\mathrm{V}^{-1}$	$0.0242462\mathrm{NV}^{-1}$

Table 2 Parameters for the double term expansion of the right hand side

i	eigenvalues $\tilde{\alpha}_i$	in-plane forces $\tilde{\tau}_i$	piezoelectric moments $\tilde{\kappa}_{Vi}$	force factors $\tilde{\kappa}_{pi}$
1	0.00051322	$\tilde{\tau}_0$	$-0.06539 + 0.2482\,\tilde{\tau}_0$	$\tilde{\kappa}_{p1}$
2	0.00098696	$0.1265 + 0.5200\,\tilde{\tau}_0$	0	0
4	0.00177653	$0.1874 + 0.2889\,\tilde{\tau}_0$	$-0.006297 + 0.02390\,\tilde{\tau}_0$	$0.02762\,\tilde{\kappa}_{p1}$

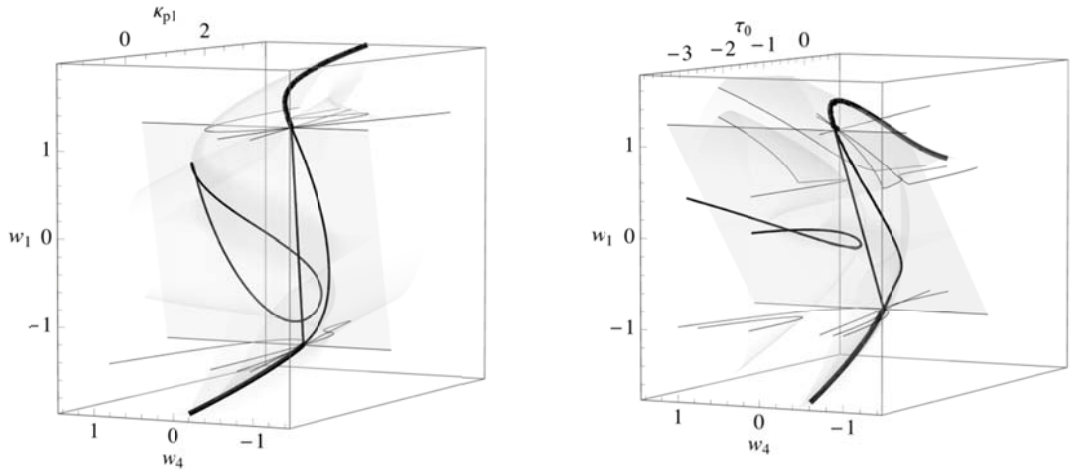

(a) $\tilde{\tau}_0 = -2.5$ (b) $\tilde{\kappa}_{p1} = 0.6$

Fig. 6 Triple term solution 3D equilibrium chart for the plate with a double term expansion of the right hand side

Here, we account for 3 terms in the solution, which correspond to the (1,1), (1,2) and (1,3) Helmholtz eigenmodes, which are the first, the second and the fourth mode; the (1,1) and the (1,3) mode are symmetric, such that $\tilde{\kappa}_{p1} \neq 0$ and $\tilde{\kappa}_{p4} \neq 0$ hold. We use the following three equations for the analysis.

$$\begin{aligned} &\tilde{w}_1\left(\tilde{\tau}_1 + \frac{1}{\tilde{\alpha}_1}\sum_{k=1,2,4}\tilde{\alpha}_k\tilde{w}_k^2\right) - \tilde{\kappa}_{V1} = \tilde{\kappa}_{p1}, \quad \tilde{w}_2\left(\tilde{\tau}_2 + \frac{1}{\tilde{\alpha}_2}\sum_{k=1,2,4}\tilde{\alpha}_k\tilde{w}_k^2\right) = 0, \\ &\tilde{w}_4\left(\tilde{\tau}_4 + \frac{1}{\tilde{\alpha}_4}\sum_{k=1,2,4}\tilde{\alpha}_k\tilde{w}_k^2\right) - \tilde{\kappa}_{V4} = \tilde{\kappa}_{p4}. \end{aligned} \tag{72}$$

From the second equation we find the equation of an ellipsoid

$$\tilde{\alpha}_1\tilde{w}_1^2 + \tilde{\alpha}_2\tilde{w}_2^2 + \tilde{\alpha}_4\tilde{w}_4^2 = -\tilde{\alpha}_2\tilde{\tau}_2, \tag{73}$$

which can be inserted into the first and the third equation. With the notion $\tilde{\tau}_1 = \tilde{\tau}_0$ the result is

$$\begin{aligned} &\tilde{w}_1\left(\tilde{\tau}_0 - \frac{\tilde{\alpha}_2}{\tilde{\alpha}_1}\tilde{\tau}_2(\tilde{\tau}_0)\right) - \tilde{\kappa}_{V1}(\tilde{\tau}_0) = \tilde{\kappa}_{p1}, \\ &\tilde{w}_4\left(\tilde{\tau}_4(\tilde{\tau}_0) - \frac{\tilde{\alpha}_2}{\tilde{\alpha}_4}\tilde{\tau}_2(\tilde{\tau}_0)\right) - \tilde{\kappa}_{V4}(\tilde{\tau}_0) = \tilde{\kappa}_{p4}(\tilde{\kappa}_{p1}). \end{aligned} \tag{74}$$

For either $\tilde{\tau}_0$ fixed or $\tilde{\kappa}_{p1}$ fixed these two equations represent a straight line in either the

$(\widetilde{w}_1, \widetilde{w}_4, \tilde{\kappa}_{p1})$-space or the $(\widetilde{w}_1, \widetilde{w}_4, \tilde{\tau}_1)$-space, which intersects the curve of the equilibrium points of solutions computed for $\widetilde{w}_2 = 0$. At these intersection points the solution branches have a bifurcation point, at which the first type of solution with $\widetilde{w}_2 = 0$ bifurcates to the second type of solution with $\widetilde{w}_2 \neq 0$ and the solution becomes unstable; again this can be referred to unstable mode jumping. Hence, the two bifurcation points define the critical equilibrium points, at which snap buckling occurs. This behaviour has been analysed for constant $\tilde{\tau}_0$ in Krommer and Irschik (2015), but the case of a constant $\tilde{\kappa}_{p1}$ is studied in the present paper for the first time. The 3D equilibrium charts are shown in Fig. 6.

Stable equilibrium branches are plotted with a solid thick line, unstable ones with a solid thin line; the straight solid thin line interconnects the two bifurcation points. In Fig. 6(a) the case $\tilde{\tau}_0 = -2.5$ is presented, for which the applied voltage is held constant, whereas the pressure is varied; in Fig. 6(b) the case $\tilde{\kappa}_{p1} = 0.6$ is presented, for which the pressure is held constant, whereas the applied voltage is varied. The analysis of the double term expansion in combination with a triple term solution already allows us to analyse and discuss the static behaviour of the specific plate under consideration for both actuation and external forces. Nonetheless, the results, which are based on assumptions like the von Karman and Tsien kinematic hypothesis and the Berger approximation, must be verified by a theory not making these assumptions. Moreover, a general theory also enables us to study more general problems with regards to geometry and material.

5. Numerical results

In this section we present numerical results computed with the Finite Element implementation presented in section 3.1 for the fully nonlinear formulation. First, the FE implementation is verified against a result reported in the literature, and secondly, the results presented in section 4 are verified with the Finite Elements.

5.1 Verification of the Finite Element implementation

To verify our geometrically fully nonlinear formulation and the corresponding Finite Element implementation, we compare our results with results reported in the literature. As an example problem a square plate made of 6 layers with a symmetric lamination scheme is studied; this problem has also been studied in Varelis and Saravanos (2002) and Klinkel and Wagner (2006). The top and bottom layer are made of *PZT-5* and the 4 core layers are made of graphite epoxy (*GE*) with the lamination scheme (0°/90°/90°/0°). The material parameters needed for the plane stress assumption in our model are reported in the Appendix. The thickness of the *GE* layers is $h_{GE}=h/8$ and the one of the *PZT-5* layers is $h_{PZT}=h/4$, with $h=1$mm for the total thickness of the plate, which has a length $L=200$mm. The 4 edges are simply supported and prevented from any in-plane displacement. An identical voltage is applied to the two piezoelectric layers, in a way that would not result into any deformation within a linear theory. In the nonlinear theory this undeformed configuration becomes unstable once the voltage reaches a critical value. In the absence of an imperfection a pitchfork bifurcation can be observed. First, we compute the critical voltage; the numerical value is presented in Tab. 3 together with the values reported by Varelis and Saravanos (2002) and Klinkel and Wagner (2006).

Table 3 Critical voltage

FE (8 × 8)	FE (16 × 16)	Varelis and Saravanos (2002)	Klinkel and Wagner (2006)
67.944V	67.943V	68.8V	70.58V

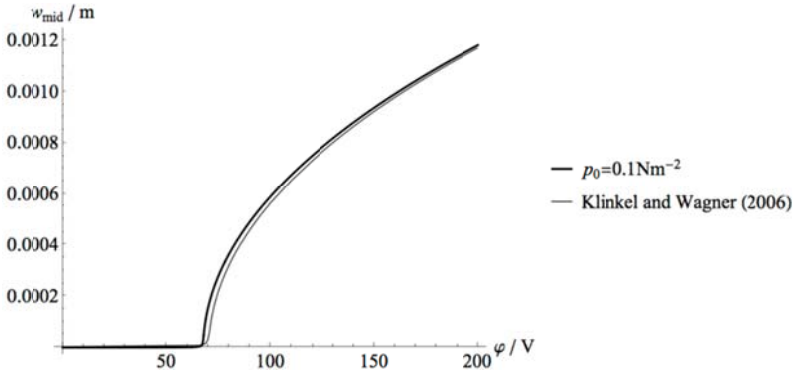

Fig. 7 Mid-point displacement of the layered plate

The computed critical voltage V_{crit}=67.943V corresponds very well with the results from the literature; the deviation from the value reported in Varelis and Saravanos (2002) (-1.266%) is less than the deviation of the one reported in Klinkel and Wagner (2006) from the one in Varelis and Saravanos (2002) (2.59%). A converged value was already obtained with 8 × 8 elements; this corresponds to the number of elements used in Varelis and Saravanos (2002). In contrast 16 × 16 elements in the plane and 6 elements through the thickness were used in Klinkel and Wagner (2006). We complete this example with the post-buckling behaviour; for that sake a small imperfection in terms of a transverse force $p_Z=p_0$=const. is imposed into the plate. Fig. 7 shows the computed mid-point deflection w_{mid} for p_0=1 Nm^{-2}; in addition the result from Klinkel and Wagner (2006) is shown as well. Again the results agree very well. Finally, we note that the imperfection was imposed as a small change in the thickness of the bottom piezoelectric layer in Klinkel and Wagner (2006).

5.2 Comparison of analytical and numerical results

To verify our analysis based on the von Karman and Tsien equation, we use the previous example. Solutions are computed for a triple term solution with a double term expansion of the right hand side (denoted by *Present* in the figures) and using the Finite Element implementation (denoted by *FE* in the figures). We study two cases. First, a constant voltage is applied and the pressure is varied; in the specific example, the voltage is either zero, for which $\tilde{\tau}_0$=0.264 is obtained, or it is non-zero, for which we have $\tilde{\tau}_0$=-0.6. The results are shown in Fig. 8.

Secondly, the pressure is held constant with either a zero pressure, $\tilde{\kappa}_{p1}$=0, or a non-zero one with $\tilde{\kappa}_{p1}$=0.15; these results are shown in Fig. 9. From the results, we conclude that the analysis carried out in this paper provides good results in comparison to a fully geometrically nonlinear theory; yet, we can also see deviations for the case the deflection goes beyond the thickness of the

plate. These deviations can be explained by the fact that the von Karman and Tsien theory is typically valid only for moderately large deformations up to the order of the thickness of the plate and by the fact that we have also used the Berger approximation. Nonetheless, the simplified theory enables the mathematical analysis of thin piezoelectric plates in the geometrically nonlinear regime, the discussion of buckling and of the post-buckling behaviour.

6. Conclusions

In the present paper three main points were addressed. First, we discussed the electromechanically coupled modelling of thin piezoelectric plates in a geometrically nonlinear regime. Both, a fully geometrically nonlinear theory and a simplified theory based on the von Karman and Tsien assumption were derived. Secondly, the von Karman and Tsien theory was used to analyse the buckling and the post-buckling behaviour of thin piezoelectric plates. Here, the important aspect of snap buckling and mode jumping was discussed for two cases; a fixed transverse force loading and a varying piezoelectric actuation as well as a fixed piezoelectric actuation and a varying transverse force loading. Thirdly, the results obtained from the mathematical analysis of the von Karman and Tsien theory were numerically verified with solutions of the fully geometrically nonlinear theory computed with Finite Elements. We consider the following points as the major findings of this paper

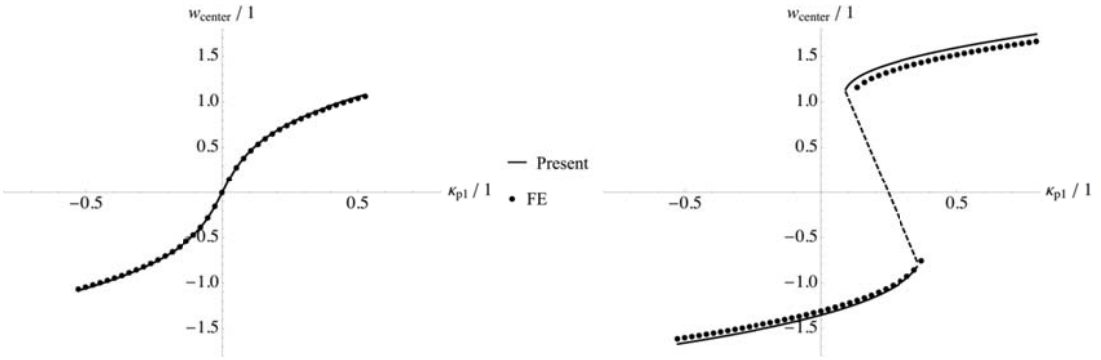

Fig. 8 Numerical results vs. analytical ones for $\tilde{\tau}_0$=0.264 (left) and $\tilde{\tau}_0$=-0.6 (right)

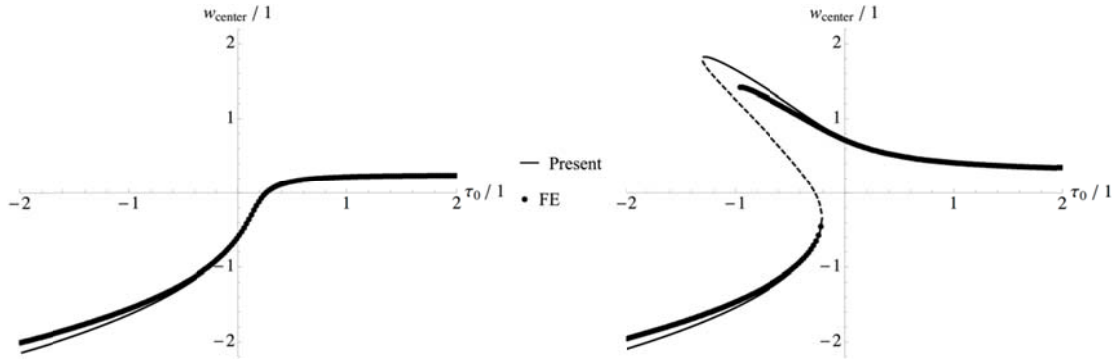

Fig. 9 Numerical results vs. analytical ones for $\tilde{\kappa}_{p1}$=0 (left) and $\tilde{\kappa}_{p1}$=0.15 (right)

- In the problems studied in this paper an applied actuator voltage results into an in-plane actuation and an actuation moment; hence, we have a non symmetric problem, for which we were able to find a transcritical bifurcation for a specific non zero value of the external transverse force loading, see Fig. 2(b). For this specific transverse force loading a solution for the deflection of the plate exists, which is independent of the actuation. Yet, this solution becomes unstable for a critical value of the actuation; at this value a transcritical bifurcation of the deflection occurs.
- The stability of equilibrium solutions of a single term expansion for the deflection must be judged by using at least a double term solution. In particular, we have found the interesting phenomenon that for a constant transverse force loading inducing a deflection in the positive direction, a snap buckling to negative deflections occurs at a critical value of the actuation, despite the fact that the actuation increases the positive value of the deflection below the critical value; see Fig. 4.
- In order to study practical problems, multi term expansions and solutions were analysed. Such solutions enable to account for multi term expansions of the transverse force loading as well as of the actuation. As before, snap buckling occurs due to mode jumping and the correct analysis of stability requires to consider expansion terms in the solution, which would be trivial in a geometrically linear theory; see Fig. 6.
- Finally, we have verified the results from the mathematical analysis of the von Karman and Tsien theory by Finite Element solutions for a fully geometrically nonlinear theory. Here, we found a good qualitative agreement between the results; see Figs. 8 and 9. Yet, the quantitative agreement was only acceptable for deflections up to the thickness of the plate. Therefore, one must conclude that the simplified von Karman and Tsien theory should only be used to analyse and discuss the buckling and the post-buckling behaviour for deflections with a magnitude close to the thickness of the plate.

Acknowledgments

This work has been supported by the Linz Center of Mechatronics (LCM) in the framework of the Austrian COMET-K2 programme.

References

Alkhatib, R. and Golnaraghi, M.F. (2003), "Active Structural Vibration Control: A Review", *Shock Vib. Dig.*, **35**(5), 367-383.

Arefi, M. and Rahimi, G.H. (2012), "Studying the nonlinear behavior of the functionally graded annular plates with piezoelectric layers as a sensor and actuator under normal pressure", *Smart Struct. Syst.*, **9**(2), 127-143.

Ashwell, D.G. (1962), "Nonlinear problems", in *Handbook of Engineering Mechanics*, (Ed., W. Flügge), McGraw Hill, New York, NY, USA.

Batra, R.C. and Vidoli, S. (2002), "Higher order piezoelectric plate theory derived from a three dimensional variational principle", *AIAA J*, **40**, 91-104.

Berger, H.M. (1955), "A new approach to the analysis of large deflections of plates", *J. Appl. Mech. - ASCE*, **77**, 465-472.

Bonet, J. and Wood, R.D. (2008), *Nonlinear Continuum Mechanics for Finite Element Analysis*, 2nd Ed.,

Cambridge University Press, Cambridge, England.
Carrera, E. and Boscolo, M. (2007), "Classical and mixed finite elements for static and dynamic analysis of piezoelectric plates", *Int. J. Numer Meth. Eng.*, **70**(10), 1135-1181.
Crawley, E.F. (1994), "Intelligent structures for aerospace: A Technology Overview and Assessment", *AIAA J.*, **32**(8), 1689-1699.
Dorfmann, A, and Ogden, R.W. (2005), "Nonlinear Electroelasticity", *Acta Mech.*, **17**, 167-183.
Eringen, A.C. and Maugin, G.A. (1990), *Electrodynamics of Continua I: Foundations and Solid Media*, Springer, New York, NY, USA.
Hause, T., Librescu, L. and Johnson, T.F. (1998), "Thermomechanical load-carrying capacity of sandwich flat panels", *J. Therm. Stresses*, **21**(6), 627-653.
Heuer, H., and Ziegler, F. (2004), "Thermoelastic stability of layered shallow shells", *Int. J. Solids Struct.*, **41**, 2111-2120.
Heuer, R. (1994), "Large flexural vibrations of thermally stressed layered shallow shells", *Nonlinear Dynamics*, **5**(1), 25-38.
Heuer, R., Irschik, H. and Ziegler, F. (1993), "Nonlinear random vibrations of thermally buckled skew plates", *Probabilist. Eng. Mech.*, **8**, 265-271.
Irschik, H. (1986), "Large thermoelastic deflections and stability of simply supported polygonal panels", *Acta Mech.*, **59**, 31-46.
Jabbaria, M., Farzaneh Joubaneha, E., Khorshidvanda A.R. and Eslamib, M.R. (2013), "Buckling analysis of porous circular plate with piezoelectric actuator layers under uniform radial compression", *Int. J. Mech. Sci.*, **70**, 50-56.
Jadhav, P.A. and Bajoria, K.M. (2012), "Buckling of piezoelectric functionally graded plate subjected to electro-mechanical loading", *Smart Mat. Struct.*, **21**(10), 105005.
Kamlah, M. (2001), "Ferroelectric and ferroelastic piezoceramics - modeling of electromechanical hysteresis phenomena", *Continuum Mech. Therm.*, **13**, 219-268.
Klinkel, S. and Wagner, W. (2006), "A geometrically non-linear piezoelectric solid shell element based on a mixed multi-field variational formulation", *Int. J. Numer Meth. Eng.*, **65**, 349-382.
Klinkel, S. and Wagner, W. (2008), "A piezoelectric solid shell element based on a mixed variational formulation for geometrically linear and nonlinear applications", *Comput. Struct.*, **86**, 38-46.
Krommer, M. (2003), "The significance of non-local constitutive relations for composite thin plates including piezoelastic layers with prescribed electric charge", *Smart Mater. Struct.*, **12**(3), 318-330.
Krommer, M. and Irschik, H. (2015), "Post-buckling of piezoelectric thin plates", *Int. J. Str. Stab. Dyn.*, **15**(7), 1540020, 21pp.
Lentzen, S., Klosowski, P. and Schmidt, R. (2007), "Geometrically nonlinear finite element simulation of smart piezolaminated plates and shells", *Smart Mater. Struct.*, **16**, 2265-2274.
Liu, S.C., Tomizuka, M. and Ulsoy, G. (2005), "Challenges and opportunities in the engineering of intelligent structures", *Smart Struct. Syst.*, **1**(1), 1-12.
Marcus, H. (1932), *Die Theorie elastischer Gewebe*, 2nd edn., Springer, Berlin, Germany.
Marinković, D., Köppe, H. and Gabbert, U. (2007), "Accurate modeling of the electric field within piezoelectric layers for active composite structures", *J. Intel. Mat. Syst. Str.*, **18**, 503-513.
Marinković, D., Köppe, H. and Gabbert, U. (2008), "Degenerated shell element for geometrically nonlinear analysis of thin-walled piezoelectric active structures", *Smart Mat. Struct.*, **17**(1), 10pp.
Nader, M. (2008), *Compensation of Vibrations in Smart Structures: Shape Control, Experimental Realization and Feedback Control*, Trauner, Linz, Austria.
Nestorović, T., Trajkov, M. and Garmabi, S. (2015), "Optimal placement of piezoelectric actuators and sensors on a smart beam and a smart plate using multi-objective genetic algorithm", *Smart Struct. Syst.*, **14**(5), 1041-1062.
Panahandeh-Shahraki, D., Mirdamadi H.R. and Vaseghi, O. (2014), "Thermoelastic buckling analysis of laminated piezoelectric composite plates", *Int. J. Mech. Mater. Des.*, **11**(4), 371-385.
Stanciulescu, I., Mitchell, T., Chandra, Y., Eason T. and Spottswood, M. (2012), "A lower bound on snap-through instability of curved beams under thermomechanical loads", *Int. J. Nonlinear Mech.*, **47**(5),

561-575.
Tan, X. and Vu-Quoc, L. (2005), "Optimal solid shell element for large deformable composite structures with piezoelectric layers and active vibration control", *Int. J. Numer Meth. Eng.*, **64**, 1981-2013.
Tani, J., Takagi, T., and Qiu, J. (1998), "Intelligent material systems: application of functional materials", *Appl. Mech. Rev.*, **51**, 505-521.
Tauchert, T.R. (1991), "Thermally induced flexure, buckling, and vibration", *Appl. Mech. Rev.*, **44**, 347-360.
Tauchert, T.R. (1992), "Piezothermoelastic Behavior of a Laminated Plate", *J. Therm. Stresses*, **15**, 25-37.
Troger, H. and Steindl, A. (1991), *Nonlinear Stability and Bifurcation Theory*, *An Introduction for Engineers and Applied Scientists*, Springer, Vienna, Austria.
Varelis, D. and Saravanos, D.A. (2002), "Nonlinear coupled mechanics and initial buckling of composite plates with piezoelectric actuators and sensors", *Smart Mat. Struct.*, **11**, 330-336.
Vetyukov, Y. (2014a), "Finite element modeling of Kirchhoff-Love shells as smooth material surfaces", *ZAMM*, **94**, 150-163.
Vetyukov, Y. (2014b), *Nonlinear Mechanics of Thin-Walled Structures: Asymptotics*, *Direct Approach and Numerical Analysis*, Springer, Vienna, Austria.
Vetyukov, Y., Kuzin, A. and Krommer, M. (2011), "Asymptotic splitting in the three-dimensional problem of elasticity for non-homogeneous piezoelectric plates", *Int. J. Solids Struct.*, **48**, 12-23.
von Karman, T. and Tsien, H.S. (1941), "The buckling of thin cylindrical shells under axial compression", *J. Aeronaut. Sci.*, **8**, 303-312.
Wu, C.P. and Ding, S. (2015), "Coupled electro-elastic analysis of functionally graded piezoelectric material plates", *Smart Struct. Syst.*, **16**(5), 781-806.
Yaghoobi, H. and Rajabi, I. (2013), "Buckling analysis of three-layered rectangular plate with piezoelectric layers", *J. Theor. Appl. Mech.*, **51**(4), 813-826.
Zenz, G., Berger, W., Gerstmayr, J., Nader, M. and Krommer, M. (2013), "Design of piezoelectric transducer arrays for passive and active modal control of thin plates", *Smart Struct. Syst.*, **12**(5), 547-577.
Zheng, S., Wang, X. and Chen, W. (2004), "The formulation of a refined hybrid enhanced assumed strain solid shell element and its application to model smart structures containing distributed piezoelectric sensors/ actuators", *Smart Mater. Struct.*, **13**, 43-50.
Ziegler, F. (1998), *Mechanics of Solids and Fluids*, 2nd edn., Springer, New York, NY, USA.
Ziegler, F. and Rammerstorfer, F.G. (1989), "Thermoelastic stability", in *Thermal Stresses III*, (Es., R.B. Hetnarski), Elsevier, Amsterdam, The Netherlands.

Appendix

For a material belonging to the crystal class 2mm with a polarization in the 3-direction (such as *PZT-5A*) the linearized three-dimensional constitutive relations can be written in matrix form as

$$\begin{bmatrix} \sigma_{11} \\ \sigma_{22} \\ \sigma_{33} \\ \sigma_{23} \\ \sigma_{13} \\ \sigma_{12} \\ D_1 \\ D_2 \\ D_3 \end{bmatrix} = \begin{bmatrix} Q_{11} & Q_{12} & Q_{13} & 0 & 0 & 0 & 0 & 0 & -e_{31} \\ Q_{12} & Q_{11} & Q_{13} & 0 & 0 & 0 & 0 & 0 & -e_{31} \\ Q_{13} & Q_{13} & Q_{33} & 0 & 0 & 0 & 0 & 0 & -e_{33} \\ 0 & 0 & 0 & Q_{44} & 0 & 0 & 0 & -e_{15} & 0 \\ 0 & 0 & 0 & 0 & Q_{44} & 0 & -e_{15} & 0 & 0 \\ 0 & 0 & 0 & 0 & 0 & Q_{66} & 0 & 0 & 0 \\ 0 & 0 & 0 & 0 & e_{15} & 0 & \eta_{11} & 0 & 0 \\ 0 & 0 & 0 & e_{15} & 0 & 0 & 0 & \eta_{11} & 0 \\ e_{31} & e_{31} & e_{33} & 0 & 0 & 0 & 0 & 0 & \eta_{33} \end{bmatrix} \begin{bmatrix} \varepsilon_{11} \\ \varepsilon_{22} \\ \varepsilon_{33} \\ \gamma_{23} \\ \gamma_{13} \\ \gamma_{12} \\ E_1 \\ E_2 \\ E_3 \end{bmatrix}; \tag{75}$$

here, the (1,2)-plane is the isotropic plane, and $Q_{66}=(Q_{11}-Q_{12})/2$ holds. For the plane stress case and for $D_1=0$ and $D_2=0$, we have $E_1=0$, $E_2=0$, $\gamma_{23}=0$ and $\gamma_{13}=0$; moreover, from $\sigma_{33}=0$ we find the effective constitutive relation as

$$\begin{bmatrix} \sigma_{11} \\ \sigma_{22} \\ \sigma_{12} \\ D_3 \end{bmatrix} = \begin{bmatrix} Y & Y\nu & 0 & -\underline{e} \\ Y\nu & Y & 0 & -\underline{e} \\ 0 & 0 & \dfrac{Y(1-\nu)}{2} & 0 \\ \underline{e} & \underline{e} & 0 & \underline{\varepsilon} \end{bmatrix} \begin{bmatrix} \varepsilon_{11} \\ \varepsilon_{22} \\ \gamma_{12} \\ E_3 \end{bmatrix}, \tag{76}$$

$$\text{with:} \quad Y = Q_{11} - \frac{Q_{13}Q_{13}}{Q_{33}}, \quad Y\nu = Q_{12} - \frac{Q_{13}Q_{13}}{Q_{33}}, \quad \underline{e} = e_{31} - \frac{e_{33}Q_{13}}{Q_{33}}, \quad \underline{\varepsilon} = \eta_{33} + \frac{e_{33}e_{33}}{Q_{33}}. \tag{77}$$

Then, the effective stiffnesses A and D, the effective Poisson ratios ν_A and ν_D and the effective actuation $\underline{\tau}$ and $\underline{\mu}$ are:

$$\begin{aligned} A &= \sum_{k=1}^{n} \int_{h^k} Y^k \, dZ, \quad \nu_A = \frac{1}{A} \sum_{k=1}^{n} \int_{h^k} Y^k \nu^k \, dZ, \quad \underline{\tau} = \sum_{k=1}^{n} \underline{e}^k V^k, \\ D &= \sum_{k=1}^{n} \int_{h^k} Z\left(Y^k Z - \frac{(\underline{e}^k)^2}{\underline{\varepsilon}^k}(Z_m^k - Z)\right) dZ, \\ \nu_D &= \frac{1}{D} \sum_{k=1}^{n} \int_{h^k} Z\left(Y^k \nu^k Z - \frac{(\underline{e}^k)^2}{\underline{\varepsilon}^k}(Z_m^k - Z)\right) dZ, \quad \underline{\mu} = \sum_{k=1}^{n} Z_m^k \underline{e}^k V^k, \end{aligned} \tag{78}$$

in which we account for $k=1,...,n$ layers. Finally, the specific material parameters for *PZT-5A* are given in Table 4.

Table 4 Material parameters for *PZT-5A* ($\varepsilon_0 = 8.854 \times 10^{-12}\mathrm{AsV^{-1}m^{-1}}$)

Elasticity moduli [$10^9\mathrm{Nm^{-2}}$]	Q_{11}	Q_{12}	Q_{13}	Q_{33}	Q_{44}	Q_{66}
	121	75.4	75.2	111	21.1	98.2
Piezoelectric coefficients [$\mathrm{Cm^{-2}}$]	e_{31}	e_{33}	e_{15}			
	-5.46	15.8	12.32			
Permittivities	η_{11}	η_{33}				
	$1730\,\varepsilon_0$	$1700\,\varepsilon_0$				

For the example problem, which is concerned with the composite plate made of four layers of *GE* and two *PZT-5* layers, the material parameters are given in Table 5.

Table 5 Material parameters for the composite plate

	$E_{11}/\mathrm{Nm^{-2}}$	$E_{22}/\mathrm{Nm^{-2}}$	ν_{12}	$G_{12}/\mathrm{Nm^{-2}}$	$d_{31}/\mathrm{mV^{-1}}$	$\varepsilon_z/\varepsilon_0$
GE (0°)	132.4×10^9	10.8×10^9	0.24	5.6×10^9	-	-
PZT-5	62×10^9	62×10^9	0.31	23.6×10^9	-220×10^{-12}	2598

From these parameters we compute the effective plane stress constitutive relation as

$$\begin{bmatrix}\sigma_{11}\\ \sigma_{22}\\ \sigma_{12}\end{bmatrix} = \underbrace{\begin{bmatrix}\underline{Q}_{11} & \underline{Q}_{12} & 0\\ \underline{Q}_{12} & \underline{Q}_{22} & 0\\ 0 & 0 & \underline{Q}_{66}\end{bmatrix}}_{=[\underline{\mathbb{C}}]}\begin{bmatrix}\varepsilon_{11}\\ \varepsilon_{22}\\ \gamma_{12}\end{bmatrix} - \underbrace{\begin{bmatrix}\underline{e}\\ \underline{e}\\ 0\end{bmatrix}}_{=[\underline{\mathbf{e}}]}E_3, \quad D_3 = \underbrace{\begin{bmatrix}\underline{e} & \underline{e} & 0\end{bmatrix}}_{=[\underline{\mathbf{e}}]^T}\begin{bmatrix}\varepsilon_{11}\\ \varepsilon_{22}\\ \gamma_{12}\end{bmatrix} + \underline{\varepsilon}E_3, \tag{79}$$

in which $[\underline{\mathbb{C}}]$ is the square matrix of Cartesian components of the effective plane stress elasticity tensor $\underline{\mathbb{C}}$, $[\underline{\mathbf{e}}]$ the column matrix of Cartesian components of the effective plane stress tensor $\underline{\mathbf{e}}$ of piezoelectric coefficients and $\underline{\varepsilon}$ is the effective plane stress permittivity. The components are defined as

$$[\underline{\mathbb{C}}] = \begin{bmatrix}1/E_{11} & -\nu_{12}/E_{11} & 0\\ -\nu_{12}/E_{11} & 1/E_{22} & 0\\ 0 & 0 & 1/G_{12}\end{bmatrix}^{\backslash 1}, \quad [\underline{\mathbf{e}}] = [\underline{\mathbb{C}}]^{-1}\begin{bmatrix}d_{31}\\ d_{31}\\ \\ 0\end{bmatrix}, \quad \underline{\varepsilon} = \varepsilon_z \tag{80}$$